Thin Solid Films 529 (2013) 242–247

Contents lists available at SciVerse ScienceDirect

Thin Solid Films

journal homepage: www.elsevier.com/locate/tsf

Sol–gel synthesis of intrinsic and aluminum-doped zinc oxide thin films as transparent conducting oxides for thin film solar cells

Shahzad Salam [a], Mohammad Islam [b,*], Aftab Akram [c]

[a] State Key Laboratory of New Ceramics and Fine Processing, Department of Material Science and Engineering, Tsinghua University, PR China
[b] Center of Excellence for Research in Engineering Materials (CEREM), Advanced Manufacturing Institute, King Saud University, P. O. Box 800, Riyadh 11421, Saudi Arabia
[c] School of Chemical and Materials Engineering, National University of Sciences and Technology, Islamabad, Pakistan

ARTICLE INFO

Available online 29 October 2012

Keywords:
Sol–gel
Al:ZnO
ZnO
Preferred orientation
Transparent conducting oxide
Van der Pauw
Band gap

ABSTRACT

Sol–gel synthesis of intrinsic (i-ZnO) and aluminum-doped zinc oxide (Al:ZnO) thin films was carried out via spin coating process using 0.2 M Zn^{2+} precursor salt, monoethanolamine to Zn^{2+} ratio of 0.75, and 1 and 2 at.% aluminum as a dopant. After annealing at 500 °C for 1 h, the structural, compositional, electrical, and optical properties of the films were investigated. Scanning electron microscope studies revealed smooth, dense film microstructure with granular cross-sectional morphology. The average grain size was in the range of 25 to 53 nm, depending on film composition, and indicated reduction in size with more Al incorporation. The processing conditions favored (002) preferential growth in all the films, with degree of preferred growth as high as 0.45, as determined from X-ray diffraction analysis. Al:ZnO film with 1 at.% Al was found to exhibit minimum resistivity value of 4.06×10^{-3} Ω cm and carrier concentration as high as 5.52×10^{19} cm^{-3}. From optical transmittance spectra, the absorption edge of the films was determined to be at ~370 nm with ≥80% transmittance in visible and near-infrared regions of the spectrum. The calculated values of band gap indicated continuous increase from 3.35 to 3.41 eV upon Al doping of the films.

1. Introduction

Transparent conductive oxides (TCOs) are binary or tertiary oxides of metals with high free carrier density, excellent electrical conductivity, and high optical transmittance in the UV–VIS-NIR spectrum. Since intrinsic, stoichiometric TCOs do not exhibit high conductivity and transmittance, such characteristics can be obtained by using appropriate dopants thus producing oxides with a non-stoichiometric composition. Thin films of cadmium oxide were reported with a yellow-orange color and a conductivity of ~10^3 S/cm [1]. Tin doped indium oxide (ITO, $Sn:In_2O_3$) is one of the most widely used TCO material, although indium being scarce is quite expensive. Due to their relatively low cost, non-toxicity, and high chemical and thermal stability, doped zinc oxides are promising materials to replace ITO in many applications [2,3].

Zinc oxide (ZnO) based TCO materials both as thin films and nanostructures, are being explored in a variety of optoelectronic devices including surface acoustic wave devices, sensor applications, photodetectors, flexible displays, optical waveguides, and transparent electrodes for solar cells [4–8]. In context with solar cell technology, TCOs are also referred to as window layer materials for their ability to transmit UV/VIS radiation through them as so to conduct electric currents with low resistive losses. ZnO is a group II–VI semiconductor with a direct band gap ($E_g = 3.37$ eV). The electronic conductivity of ZnO is attributed to the ionized Zn interstitial atoms and the electrons produced, due to vacancies within the crystal structure. An appropriate dopant, up to a certain concentration level, can act as an electron donor to the conduction band in ZnO thus increasing its electrical conductivity. Depending on the nature of the dopant, ZnO can be made an n- or p-type semiconductor.

The electronic properties of ZnO can be improved by doping it with any of the elements belonging to the groups III A (Al, Ga, In), IV A (Si, Ge), and IV B (Ti, Zr, Hf) of the periodic table [9]. Although both intrinsic and doped ZnO films have been produced using various thin film deposition techniques, sputtering is the most commonly used processing route explored. Sputter deposited and vacuum annealed Bi-doped ZnO films exhibited electrical resistivity and carrier concentration of 1.89×10^{-3} Ω cm and 3.45×10^{20} cm^{-3}, respectively [10]. Malinovska et al. [11] reported a minimum electrical resistivity of 1.6×10^{-3} Ω cm for r.f. magnetron sputtered V-doped ZnO films with vanadium concentration of 1.41 at.%. Recently, a significant drop in electrical resistivity with associated increase in carrier concentration and mobility was reported for magnetron sputtered Ga-doped ZnO films produced at high temperatures [12]. For sub-micron thick Al-doped ZnO (AZO) films, r.f. magnetron sputtering indicated a decreasing trend in electrical resistivity with increasing thickness [13].

Due to its simplicity, low cost, and easy-to-control processing parameters, sol–gel method is being extensively explored as a promising alternative route to vacuum based deposition techniques for

* Corresponding author.
E-mail addresses: miqureshi@ksu.edu.sa, mohammad.islam@gmail.com (M. Islam).

0040-6090/$ – see front matter
http://dx.doi.org/10.1016/j.tsf.2012.10.079

high quality ZnO films. Using inorganic (nitrates, perchlorates, chlorides) or organic salts (acetates, acetylacetonates) in alcohols, initial in-situ formation of alkoxide or alkoxy-complexes is followed by oxide formation via hydrolysis and polymerization reactions. Using this technique, In-doped ZnO films produced under optimal film thickness and annealing conditions had the minimum electrical resistivity of 1.3×10^{-2} Ω cm [14]. Although the electrical resistivity of sol–gel AZO films is of the order of 10^{-3} Ω cm, it is still higher than their counterparts produced using vacuum based techniques by one order of magnitude [15,16].

In this paper, we report results from sol–gel synthesis of intrinsic and Al-doped ZnO thin films. The precursor sol containing 0.2 M Zn^{2+} and MEA:Zn^{2+} in a ratio of 0.75 was used to produce ZnO and Al-doped ZnO thin films via spin coating process. For each sample, films were deposited over soda-lime glass substrates in three deposition cycles followed by annealing at 500 °C in air. The composition, structure, and morphology of the films were investigated using X-ray diffraction (XRD), scanning electron microscope (SEM), high resolution transmission electron microscope (HRTEM) and atomic force microscope (AFM) techniques. Electrical and optical properties were determined by means of Hall effect measurements and UV–VIS-NIR spectroscopy, respectively.

2. Experimental details

2.1. Substrate pre-treatment and solution preparation

For deposition of intrinsic and doped zinc oxide thin films, small sectioned coupons of soda-lime glass, 10×10 mm in size, were used as substrates. The substrates were cleaned using 2 wt.% chromic acid solution, then washed with methanol and finally thoroughly rinsed in excess of de-ionized water. The sol solution prepared for spin coating onto substrates had the following constituents: zinc acetate dehydrate (ZAD) $Zn(CH_3COO)_2\cdot2H_2O$, monoethanolamine (MEA) $(HOCH_2CH_2)NH_2$, iso-propanol (i-PrOH) $(CH_3)_2CHOH$, aluminum chloride hexahydrate $AlCl_3\cdot6H_2O$, and ethanol (EtOH) CH_3CH_2OH. All the reagents used were of analytical grade purity (>99.99%). A 0.2 M solution was made by dissolving, ZAD as zinc precursor salt into i-PrOH followed by drop-by-drop addition of MEA to it as a stabilizer until MEA:Zn^{2+} ratio of 0.75 was achieved. The resulting mixture solution was magnetically stirred at 60 °C for 1 h until initially opaque solution transformed into transparent solution due to complete dissolution of zinc oxide powder. The solution was allowed to age for 24 h at room temperature. For Al doping, a 0.2 M solution of $AlCl_3\cdot6H_2O$ in EtOH was prepared separately with certain amount of it added to ZAD sol in such a way that precursor sol solutions with required Al content of 1 at.% and 2 at.% ([Al]/([Al]+[Zn])×100) were obtained.

2.2. Film deposition and annealing

The precursor sol solution was deposited over substrates via spin coating at spin speed of 2000 rpm for 15 s. The coated substrates were dried in a laboratory oven at 200 °C for 10 min in order to remove organic residues. In order to produce films with reasonable thickness, each cycle comprising of deposition and drying steps was repeated three times, after which the samples were annealed at 500 °C for 1 h in air ambient. The processes of solution preparation and film deposition are illustrated in Fig. 1. Thin film of pure zinc oxide as well as doped with 1 and 2 at.% Al composition were prepared.

2.3. Characterization

The films were thoroughly characterized for structure and surface morphology. For XRD studies, an X-ray diffractometer (STOE Stadi MP) was employed at operating voltage and current of 40 kV and 20 mA, respectively. The Cu-kα radiation was used as source for

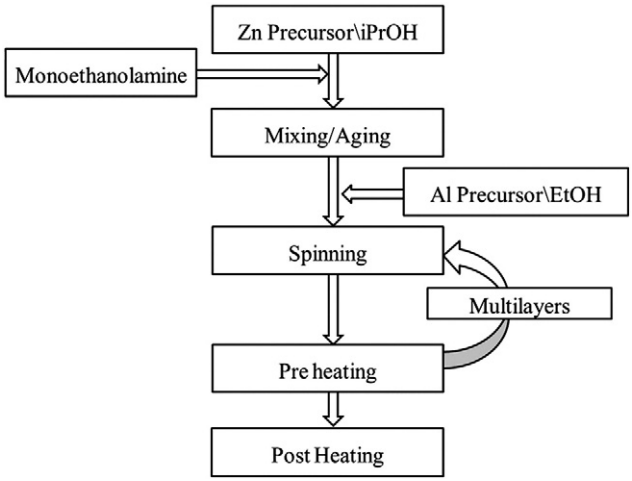

Fig. 1. Schematic illustration of sol precursor solution preparation and thin film deposition.

incident monochromatic X-ray beam, while step size and dwell time were kept at respective values of 0.04° and of 3 s per step. The average crystallite size was determined using Scherrer's equation ($t=0.94\lambda/\beta_{1/2}\cos\theta$) where λ is 0.154 nm and $\beta_{1/2}$ is full width at half maximum obtained from XRD pattern. The degree of (002) orientation was calculated by taking into consideration the intensities of (002), (100), and (101) planes in the diffraction pattern. For surface and cross-sectional examination, SEM (JEOL JSM6490A) was operated at voltage, spot size, and working distance of 20 kV, 35 or 40 nm, and 10 mm, respectively. The AFM studies were performed in air through operation in a tapping mode to maximize the tip–sample interactions. The probes used were micro-fabricated cantilevers (NSC35; μmasch) with respective values of length, nominal tip radius, spring constant, and resonance frequency to be 130 mm, <10 nm, 4.5 N/m, and 150 kHz. HRTEM was performed using a Hitachi HNAR9000 microscope with accelerating voltage of 300 kV, LaB6 electron gun and 0.18 nm point-to-point resolution. For TEM measurements, the films were examined by scratching the film and collecting a small fraction of the powder onto copper grid. Functional properties such as optical transmittance and band gap values were determined using Spectrophotometer (Labomed UV 2500), while electrical characteristics such as resistivity, carrier concentration, and carrier mobility were measured using Van der Pauw variable temperature Hall Effect measurement system (Ecopia HMS-5000). The optical band gap value (E_g) of the films can be computed through extrapolation of the $(\alpha h\nu)^2$ versus $h\nu$ curve, since photon energy is E_g when $(\alpha h\nu)^2$ becomes zero. For that purpose, the value of optical absorption coefficient (α) is calculated using film thickness, transmittance and reflectance data using mathematical correlation between these parameters [17].

3. Results and discussion

3.1. Microstructural analysis

SEM examination of the film surfaces revealed granular morphology with slight variation in average surface roughness and grain size from one sample to the other. The films were found to be polycrystalline in nature with each grain formed due to agglomeration of multiple crystallites, as suggested by X-ray diffraction analysis, described in the next section. The surface microstructures of the films at high magnification are presented in Fig. 2. The deposited films were highly dense, granular and compact in nature. From SEM images, the average grain size for intrinsic, 1 at.% Al- and 2 at.% Al-doped zinc oxide films was estimated to be ~53, 42, and 25 nm, respectively with standard deviations not exceeding 3% of the average value. Upon doping with

aluminum, there is a gradual decrease in grain size, which is consistent with an earlier report [2]. The addition of Al^{3+} ions to Zn^{2+} sol solution increases the number of nucleation sites on the substrate, thus resulting in a greater degree of preferential alignment exhibited by smaller grains subsequently giving rise to more dense film structure. The thickness and growth morphology of the films produced were examined, as shown in Fig. 3. The thickness uniformity over a large substrate area was confirmed through extensive inspection of the entire film cross-section. The film with 1 at.% Al was found to be ~300 nm thick with dense, granular cross-sectional morphology,

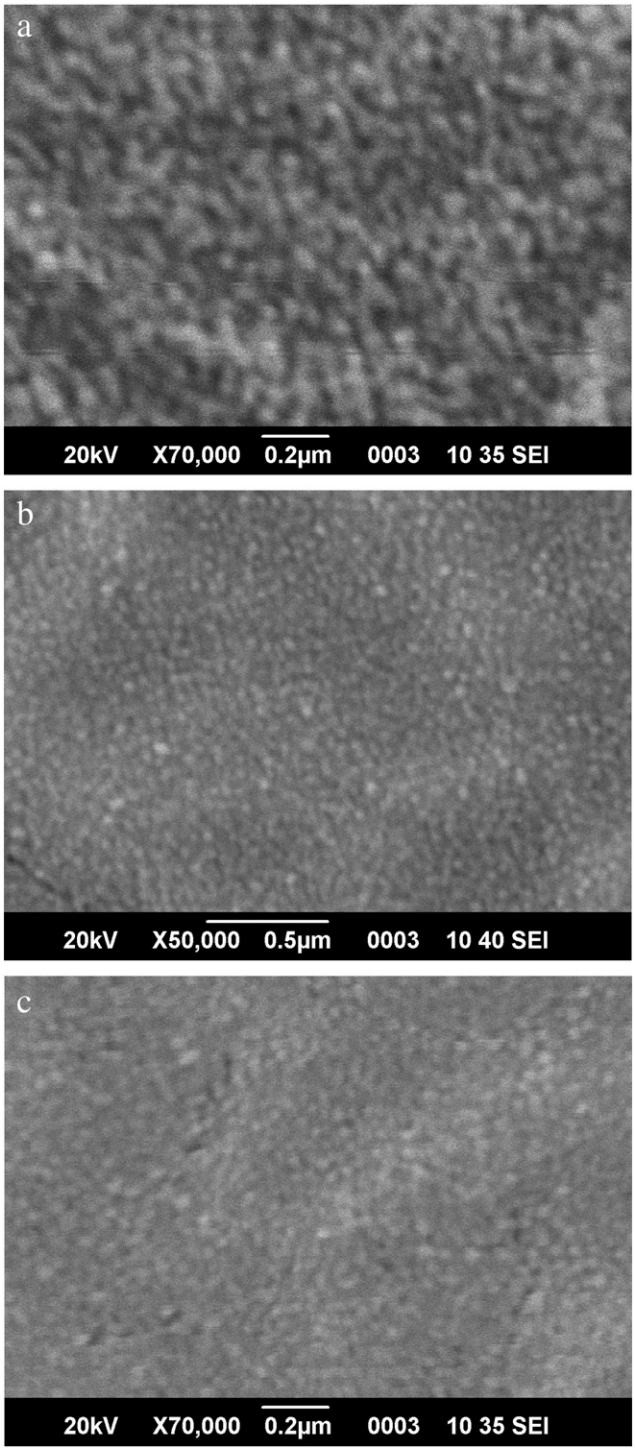

Fig. 2. SEM micrographs of AZO films; (a) un-doped (b) 1 at.% Al-doped, and (c) 2 at.% Al-doped.

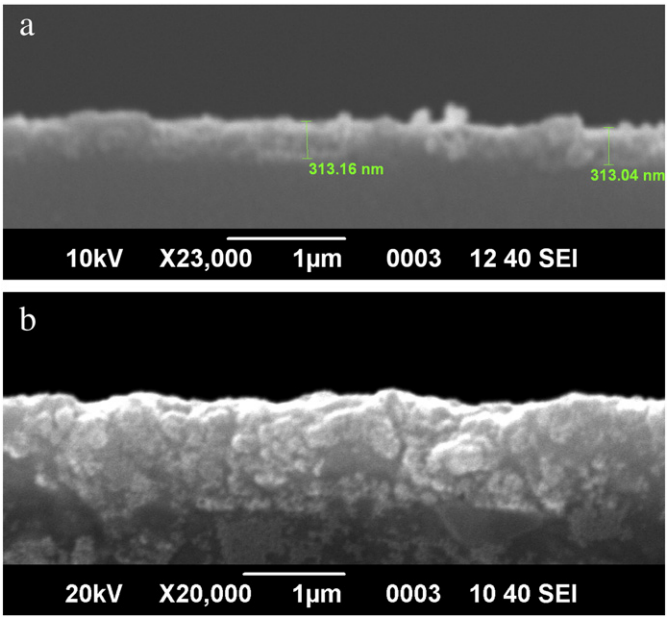

Fig. 3. High magnification SEM microstructure of film cross-sections: (a) 1 at.% Al-doped ZnO prepared from 3 coating cycles, and (b) i-ZnO film produced after 10 deposition cycles.

implying that each deposition cycle produced approximately 100 nm thick film. The presence of small amounts of Al did not have any profound effect on film growth rate, as manifested by cross-sectional examination of ZnO film produced from 10 deposition cycles, shown in Fig. 3b.

The 2-dimensional surface topography of the film is represented in a 6×6 μm size AFM scan of the 1 at.% Al-doped zinc oxide film, as shown in Fig. 4a. The degree of surface roughness as manifested by root mean square (RMS) values was determined during AFM studies and was found to decrease upon doping with aluminum (Table 1). For i-ZnO film, the HRTEM examination confirmed the polycrystalline nature of the film. As shown in Fig. 4b, high magnification microstructure revealed presence of round-shaped crystallites with distinct lattice structure formed due to diffraction from certain crystallographic planes.

3.2. Composition and phase analysis

XRD studies confirmed the crystallographic structure of both intrinsic and doped zinc oxide films to be Wurtzite ZnO. The respective XRD patterns for 2θ values in the range of 25 to 70° are shown in Fig. 5. The major peaks were indexed to be from (100), (002), and (101) planes using standard data (JCPDS 36-1451). Since the relative intensity of the (002) peak was stronger than the other peaks, the films exhibit preference towards the c-axis orientation. The reason for such preferred growth is relatively low surface energy for (002) plane, causing higher growth rate along the c-axis than other crystallographic orientations [3]. With increase in Al doping level, a corresponding decrease in crystallinity was noticed primarily because of Al segregation at grain boundaries. Another reason may be due to greater extent of oxygen capture by Al^{3+} ions than Zn^{2+} due to its larger nuclear charge. The ionic radius of aluminum (0.56 Å) is smaller than that of zinc (0.74 Å) and excess Al may also occupy interstitial positions in ZnO lattice resulting in distorted crystal structure, thus decreasing the carrier mobility [18]. The absence of any peaks characteristic of Al_2O_3 or zinc spinel ($ZnAl_2O_4$) phases indicates interstitial substitution of Zn^{2+} by Al^{3+} to be the predominant effect of Al doping and Al segregation to grain boundary region as another possibility especially for 2 at.% Al-doped ZnO films.

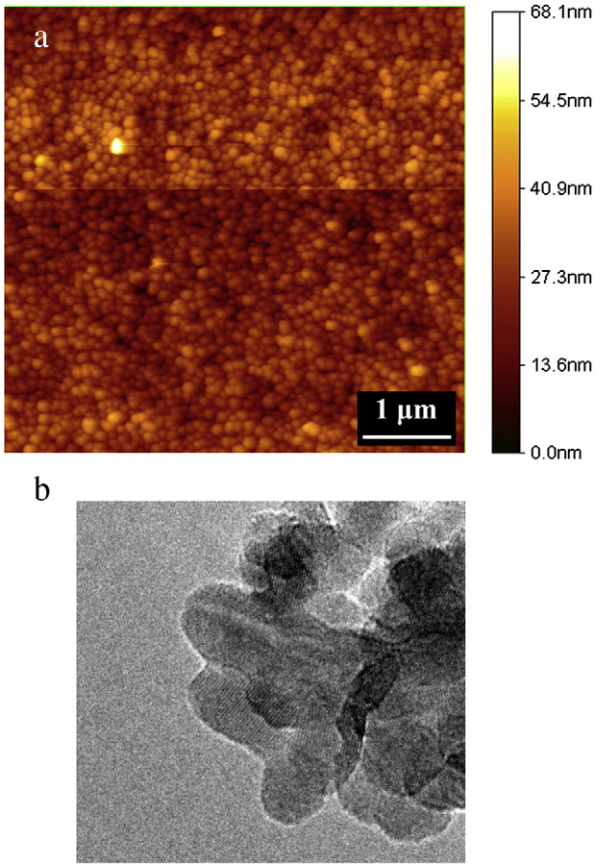

Fig. 4. (a) A 2-dimensional AFM image of the annealed film with 1 at.%Al:ZnO composition, and (b) high magnification HRTEM microstructure of the i-ZnO film. The scale bar represents a length of 5 nm.

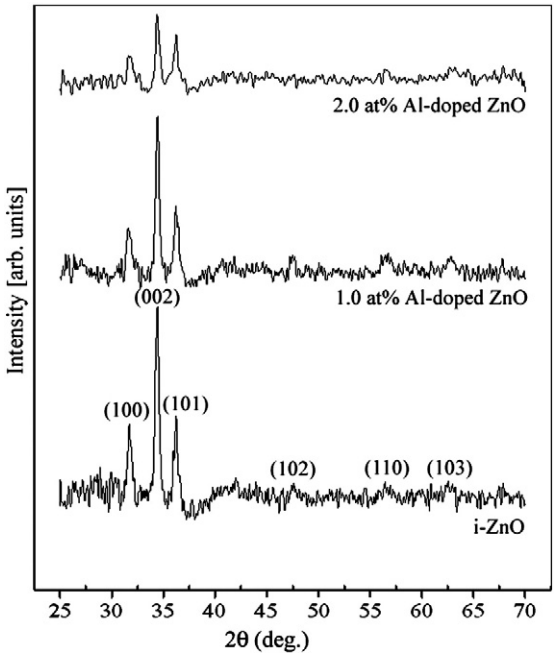

Fig. 5. The X-ray diffraction patterns for intrinsic and Al-doped ZnO films after annealing in air at 500 °C for 1 h.

The crystallite size of the annealed films was calculated using Scherrer formula by taking into consideration full-width at half maximum value of the peak with maximum intensity. The values so computed were not very different for all the samples, and hence any correlation between film composition and the crystallite size cannot be established. Among other properties, the values of crystallite size for different films are listed in Table 1.

Using the formula proposed by Lotgering [19], the degree of (002) preferred orientation f_{002} in the annealed films was computed, as presented in Table 1. For this purpose, the (002) peak intensity as well as the sum of the intensities from all peaks, from recorded diffraction data and the standard card (JCPDS 36-1451), were utilized in a set of mathematical equations. The preferential orientation of sol–gel ZnO films depends on various factors namely, the choice of substrates, chemical system used (precursor salt type and its concentration, solvent, additive, aging time), film deposition technique and process parameters, and post-synthesis heat treatment conditions [20]. The (002) orientation in ZnO thin films is the kinetically preferred one that also exhibits a higher degree of grain-packing [21]. To sum it up, the precursor sol solution with 0.2 M Zn^{2+} and MEA:Zn^{2+} ratio of 0.75 produced films with much finer crystallite size and preferred orientation of (002). Although the degree of preferred orientation was in excess of 0.40 for both i-ZnO and 1 at.% AZO films, its value dropped significantly when Al doping level was increased to 2 at.%.

3.3. Electrical characteristics

The electrical properties of Al-doped ZnO films strongly depend on carrier concentration, which in turn, depends on contributions from Al^{3+} on substitutional sites of Zn^{2+} ions, Al and Zn interstitial atoms, and oxygen vacancies. The intrinsic zinc oxide (i-ZnO) films showed electrical resistivity of the order of 2.0×10^{2} Ω cm. Upon doping with 1 at.% Al, the electrical resistivity was found to decrease drastically. This is due to increased carrier concentration as a result of substitution of Zn^{2+} by Al^{3+} at lattice sites. Due to limited solubility of Al in ZnO, doping of Al beyond 1 at.% causes an increase in electrical resistivity since, instead of replacement of Zn^{2+} by Al^{3+}, excess Al^{3+} ions form nonconductive Al_2O_3 or $ZnAl_2O_4$ phases. It is, therefore, anticipated that in the case of 2 at.% Al-doped ZnO films, excess Al atoms tend to segregate at the grain boundary region causing a

Table 1
Physical properties of intrinsic and Al-doped zinc oxide films after annealing.

Properties		Film composition		
		i-ZnO	1 at.%Al:ZnO	2 at.%Al:ZnO
Structural	Film thickness (nm)	311	313	330
	Root mean square (RMS) roughness (nm)	10.3	6.5	4.2
	Crystallite size (nm)	30	33	28
	Degree of (002) orientation	0.419	0.454	0.318
Electrical	Resistivity (Ω cm)	1.97×10^{2}	4.06×10^{-3}	2.38×10^{-2}
	Carrier concentration (cm^{-3})	7.63×10^{14}	5.52×10^{19}	1.52×10^{19}
	Carrier Mobility (cm^2/Vs)	41.6	27.8	17.3
Optical	Transmittance (%)	82–85	80–85	70–75
	Band gap (eV)	3.35	3.39	3.41

drop in carrier mobility due to scattering and grain boundary potential effects.

Upon Al doping, the carrier concentration increases to a maximum value of 5.52×10^{19} cm^{-3} with an associated decrease in carrier mobility. A minimum resistivity of 4.06×10^{-3} Ω cm is measured for films with 1 at.% Al which increases to 2.38×10^{-2} Ω cm for 2 at.% Al doping. An increase in Al doping level to 2 at.% leads to deterioration in crystalline quality due to lattice strain arising from size difference between Al and Zn, oxidation of Al leading to Al_2O_3 or $ZnAl_2O_4$ formation, and less effective electron donor effect. Lattice defects induced through Al addition and Al segregation at grain boundaries have an overall effect of decrease in carrier mobility. Thus, many factors including oxidation of Al to form Al_2O_3, segregation of Al atoms to the grain boundaries, and occupation of Al atoms at interstitial sites, may have been responsible for deterioration of electrical properties.

The minimum resistivity value obtained in our work is lower than those reported in the literature [22,23], although it can be further improved through introduction of a pre heat-treatment cycle, and ensuring controlled atmosphere during annealing [17]. The values of electrical resistivity, carrier concentration, and carrier mobility for different film compositions are presented in Fig. 6. The lines are drawn merely as guides for the eyes, and by no means represent any particular correlation between film composition and electrical properties.

3.4. Optical properties

The optical transmittance spectra for all the films after annealing are presented in Fig. 7. In general, the films exhibit good transmittance with maximum value in the range of 80 to 85%T. It is evident that the average transmittance of 1 at.% Al-doped ZnO film is higher than the intrinsic ZnO film in the wavelength range of 400–600 nm which is consistent with the reported literature [24]. It is speculated that higher transparency of 1 at.% Al doped ZnO is perhaps due to more voids present in the deposited films than those doped with 2 at.% Al. In the case of intrinsic and Al-doped ZnO films, a significant reduction in %T was noticed in the near infrared (IR) region of the wavelength range. The IR regime possesses low energy as compared to the band gap values for ZnO films. Also, there is a large difference between wavelength of light in that range and length of structural features such as pore size, grain size and surface roughness values. Both factors lead to reduction in the degree of interaction between IR radiation and the film causing reflection of the light as reported in another study [25].

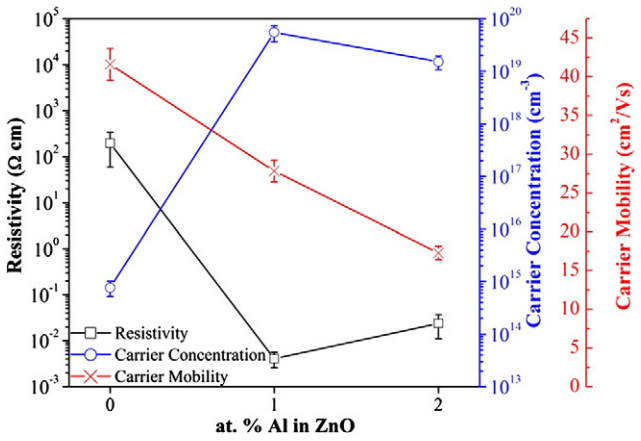

Fig. 6. Resistivity, carrier concentration, and carrier mobility of intrinsic and Al-doped ZnO films as a function of Al concentration. The error bars represent standard deviation of 5 measurements on each sample.

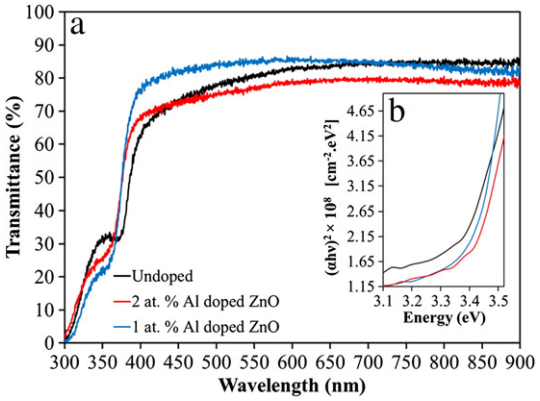

Fig. 7. Optical transmittance spectra of intrinsic and doped zinc oxide films with inset representing plot of $(\alpha h\nu)^2$ versus $h\nu$ for band gap determination.

The fundamental absorption edge lies around the wavelength of 370 nm. Furthermore, a large shoulder peak in the range of 330–370 nm is visible in the transmission spectra. The presence of this excitonic peak confirms the nanoscale size of the crystallites, since these nanocrystals give rise to the quantum confinement effect. From Fig. 7a, a blue shift in the absorption edge is noticed upon doping with Al which is indicative of widening of the optical band gap energy as explained by Burstein–Moss theory. In the case of heavily doped ZnO films, a donor level is generated at the base of conduction band. According to Pauli principle, a state cannot be doubly occupied and thus, the electrons in valence shell require an additional energy in order to be excited to higher states of conduction band, causing optical band gap widening.

From the graphical form of $(\alpha h\nu)^2$–$h\nu$ data presented in Fig. 7b, the E_g values were estimated and listed in Table 1. The value of band gap energy is found to increase from 3.35 to 3.41 eV upon doping with Al. The calculated values are close to those reported earlier [23,26]. The main reason for relatively low E_g values for sol–gel ZnO films than those produced using physical processes such as sputtering [27,28] is less number of localized donor levels in the energy band gap.

4. Conclusions

Sol–gel ZnO thin films are prepared using spin coating process over soda-lime glass substrates. SEM, HRTEM, and AFM studies of the films indicate them to be of sub-micron thickness with dense, granular and crack-free morphology, and polycrystalline with crystallite size of ~30 nm. The addition of Al into ZnO films decreases the average surface roughness and increases the degree of (002) preferred crystallographic orientation. Further increase in the Al doping level to 2 at.% causes lattice distortion due to the size difference between Al and Zn along with a slight drop in the (002) preferred texturing.

Upon 1 at.% Al doping, the value of electrical resistivity decreases to 4.06×10^{-3} Ω cm due to higher carrier concentration despite a slight drop in carrier mobility. Further increase in the Al doping level to 2 at.%, however, introduces lattice defects beside segregation of Al to the grain boundary area that limits electron transport through it, causing a significant drop in carrier mobility and an associated rise in the electrical resistivity value. X-ray diffraction pattern do not yield any evidence of Al_2O_3 or $ZnAl_2O_4$ phase formation for this doping level.

The optical transmittance of the intrinsic and 1 at.% Al-doped ZnO films is up to 85% which is reduced to ~75% for 2 at.% Al-doped ZnO possibly due to electron donor centers. The band gap energy of films increases from 3.35 to 3.41 eV upon Al doping in accordance with Burstein–Moss effect. Based on these findings, further optimization

of Al doping level around 1 at.% level is in progress. Sol–gel synthesis of intrinsic and Al-doped ZnO thin films is a promising avenue for simple, cost-effective alternative processing route for CIGS based thin film solar cells.

Acknowledgments

The work has been funded by the Higher Education Commission (HEC), Pakistan through the National Research Program for Universities (Grant no. 20-1603), and the National University of Sciences and Technology (NUST), Islamabad.

References

[1] M. Grundmann, H. Frenzel, A. Lajn, M. Lorenz, F. Schein, H. von Wenckstern, Phys. Status Solidi A 207 (6) (2010) 1437.
[2] M. Dutta, S. Mridha, D. Basak, Appl. Surf. Sci. 254 (2008) 2743.
[3] U. Yogeswaran, S.-M. Chen, Sensors 8 (2008) 290.
[4] W.-L. Lu, P.-K. Hung, C.-I. Hung, C.-H. Yeh, M.-P. Houng, Mater. Chem. Phys. 130 (2011) 619.
[5] Z.L. Pei, X.B. Zhang, G.P. Zhang, J. Gong, C. Sun, R.F. Huang, L.S. Wen, Thin Solid Films 497 (1–2) (2006) 20.
[6] H.K. Park, J.-W. Kang, S.I. Na, D.-Y. Kim, H.-K. Kim, Sol. Energy Mater. Sol. Cells 93 (2009) 1994.
[7] D.C. Look, In: C. Jagadish, S. Pearton (Eds.), Doping and Defects in ZnO, in Zinc oxide: Bulk, thin films, and nanostructures, Elsevier Ltd., 2006, p. 23.
[8] M. Jiang, X. Liu, H. Wang, Surf. Coat.Technol. 203 (2009) 3750.
[9] H.T. Cao, Z.L. Pei, J. Gong, C. Sun, R.F. Huang, L.S. Wen, Surf. Coat. Technol. 184 (2004) 84.
[10] D.-H. Lee, K. Kim, Y.S. Chun, S. Kim, S.Y. Lee, Curr. Appl. Phys. 12 (2012) 1586.
[11] K. Lovchinov, O. Angelov, H. Nichev, V. Mikli, D. Dimova-Malinovska, Energy Procedia 10 (2011) 282.
[12] E.J. L.-Arredondo, A. Maldonado, R. Asomoza, D.R. Acosta, M.A. M.-Lira, M. de la L. Olvera, Thin Solid Films 490 (2005) 132.
[13] M.M. Islam, S. Ishizuka, A. Yamada, K. Matsubara, S. Niki, T. Sakurai, K. Akimoto, Appl. Surf. Sci. 257 (2011) 4026.
[14] F.-H. Wang, H.-P. Chang, C.-C. Tseng, C.-C. Huang, H.-W. Liu, Curr. Appl. Phys. 11 (2011) S12.
[15] J.I. Pankove, in: Prentice-Hall Inc., New Jersey, 1971, p. 320.
[16] M. Çopuroğlu, S. O'Brien, G.M. Crean, Thin Solid Films 517 (2009) 6323.
[17] Y.-K. Tseng, G.-J. Gao, S.-C. Chien, Thin Solid Films 518 (2010) 6259.
[18] R.B.H. Tahar, J. Eur. Ceram. Soc. 25 (2005) 3301.
[19] F.K. Lotgering, J. Inorg. Nucl. Chem. 9 (2) (1959) 113.
[20] L. Znaidi, Mater. Sci. Eng. B 174 (2010) 18.
[21] C.-Y. Tsay, K.-S. Fan, Y.-W. Wang, C.-J. Chang, Y.-K. Tseng, C.-K. Lin, Ceram. Int. 36 (2010) 1791.
[22] C.M. Muiva, T.S. Sathiaraj, K. Maabong, Ceram. Int. 37 (2011) 555.
[23] W.-J. Chen, W.-L. Liu, S.-H. Hsieh, Y.-G. Hsu, Procedia Eng. 36 (2012) 54.
[24] H.-m. Zhou, D.-q. Yi, Z.-m. Yu, L.-r. Xiao, J. Li, Thin Solid Films 515 (2007) 6909.
[25] A.Y. Oral, Z.B. Bahşi, M.H. Aslan, Appl. Surf. Sci. 253 (2007) 4593.
[26] S.W. Xue, X.T. Zu, W.G. Zheng, M.Y. Chen, X. Xiang, Phys. B: Condens. Matter 382 (2006) 201.
[27] F.-H. Wang, H.-P. Chang, C.-C. Tseng, C.-C. Huang, Surf. Coat.Technol. 205 (2011) 5269.
[28] D.D. Malinovska, O. Angelov, H. Nichev, M. Kamenova, J.C. Pivin, J. Optoelectron. Adv. Mater. 9 (2007) 2512.